Sideband Generation Using Strongly Driven Raman Coherence in Solid Hydrogen

J. Q. Liang, M. Katsuragawa, Fam Le Kien,* and K. Hakuta

Department of Applied Physics and Chemistry, and Institute for Laser Science, University of Electro-Communications, Chofu, Tokyo 182-8585, Japan

CREST, Japan Science and Technology Corporation (JST), Chofu, Tokyo 182-8585, Japan

(Received 7 March 2000)

Parametric Raman sideband generation is investigated using strongly driven Raman coherence in solid hydrogen. We show that the Raman coherence prepared with two coaxial single-mode lasers beats with multimode laser radiation with very broad bandwidth and efficiently replicates the broadband nature to the Raman sidebands without the restriction of phase matching. We demonstrate that this efficient replication occurs mainly on the negative side of Raman detuning, where the medium adiabatically follows the antiphased state.

PACS numbers: 42.50.Gy, 42.50.Hz, 42.65.Ky, 42.79.Nv

There has been increasing interest in nonlinear optics using electromagnetically induced transparency (EIT) [1]. This effect allows us to efficiently generate a parametric sideband without the restriction of phase matching using a large coherence [2]. Harris and his collaborators demonstrated efficient parametric up-conversion within one coherence length using Pb vapor [3]. Zibrov *et al.* demonstrated an efficient parametric process in cw operation using a hyperfine transition in Rb atom [4]. Although the idea of EIT had been started for the resonant Raman three-level systems, the idea has now been extended to far-off-resonance Raman systems. Harris and Sokolov proposed a method to realize a large Raman coherence using adiabatic preparation with two strong driving laser pulses; they showed for molecular H_2 gas that the strongly driven molecular vibration may collinearly generate the multiorder Raman sidebands that may lead to subfemtosecond light pulse generation [5]. Yavuz *et al.* theoretically demonstrated the existence of eigenvectors for the far-off-resonance Raman system [6]. Regarding experiments, Hakuta *et al.* reported collinear parametric Raman sidebands in stimulated Raman scattering (SRS) using solid hydrogen [7]. Recently, Sokolov *et al.* have reported the collinear multiorder SRS sidebands using a strongly driven Raman coherence in D_2 gas [8].

In the present Letter, we show for the far-off-resonance Raman scheme using solid hydrogen that the Raman coherence strongly driven by two coaxial single-mode lasers parametrically beats with multimode laser radiation with a very broad bandwidth of about 300 cm^{-1}, efficiently generates the collinear Raman sidebands without the restriction of phase matching, and exactly replicates the broadband nature of the multimode laser to the sidebands. If one assumes a conventional parametric process seriously restricted by phase matching, there would be no way to generate efficiently the collinear parametric sidebands using such broadband radiation, and moreover, even assuming the resonant EIT scheme [3,4], one cannot realize such broadband replication, because the Raman coupling strength should change drastically in the resonant scheme for such a broad bandwidth of 300 cm^{-1}. We show also that the efficient parametric sideband generation occurs mainly on the negative side of Raman detuning, where the medium may adiabatically follow the antiphased state.

First, we summarize some main features of solid hydrogen. Solid hydrogen is the simplest molecular crystal consisting of H_2 molecules. Its remarkable feature is that molecules consisting of the solid have well-defined vibrational and rotational quantum states as free molecules in the gas phase and their characteristic frequencies are almost equal to the gas phase values [9]. Moreover, the spectral widths for the transitions are very narrow [10]. Regarding the pure vibrational transition $Q_1(0)$ ($v = 1 - 0$, $J = 0 - 0$), Li *et al.* measured the dephasing rate and showed that the Raman dephasing rate may become as slow as 1.5 MHz or less [11]. Katsuragawa and Hakuta reported a Raman gain measurement and showed that, regarding the Raman transition, solid hydrogen can simply be modeled as a noninteracting H_2 system with a solid number density of 2.64×10^{22} cm^{-3} [12].

Next, we estimate how large coherence should be prepared for the efficient parametric Raman sideband generation without the restriction of phase matching. The Raman coherence ρ_{ab} is prepared by driving with two single-mode pulsed lasers at $\omega_0^{(p)}$ and $\omega_{-1}^{(p)}$ between states $|a\rangle$ and $|b\rangle$, corresponding to the $Q_1(0)$ transition with energy separation 4149.64 cm^{-1}, and a beating radiation field $\mathcal{E}_0^{(\mathrm{in})}(\tau)$ at ω_0 is applied to the prepared coherence; see the inset of Fig. 1. By restricting the discussions to 1st Stokes (ω_{-1}) and anti-Stokes (ω_{+1}) sidebands and neglecting the phase slip due to dispersion, one can readily solve the propagation equations. Results are summarized below together with the phase-slip coefficient $\Delta\kappa$:

$$\mathcal{E}_i(z,\tau) \propto \mathcal{E}_0^{(\mathrm{in})}(\tau)\sin(sz), \tag{1}$$

$$s = \frac{\mathcal{N}\hbar}{\epsilon_0 c}|\rho_{ab}|\sqrt{\omega_0(\omega_1|d_0|^2 + \omega_{-1}|d_{-1}|^2)}, \tag{2}$$

 0031-9007/00/85(12)/2474(4)$15.00 © 2000 The American Physical Society

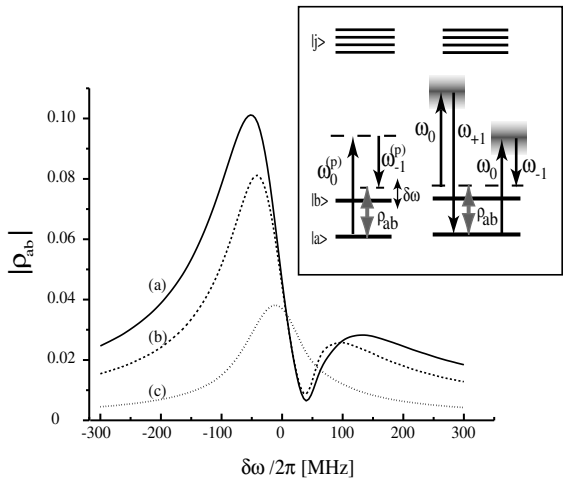

FIG. 1. Coherence versus Raman detuning calculated at a propagation distance of 100 μm for three driving intensities: (a) 180 MW/cm^2, (b) 130 MW/cm^2, and (c) 40 MW/cm^2. The inset shows the scheme for the Raman sideband generation. Two lasers at $\omega_0^{(p)}$ and $\omega_{-1}^{(p)}$ drive the Raman coherence, and the coherence beats with a laser field at ω_0 with broad bandwidth and generates sidebands at ω_1 and ω_{-1}. Upper states $|j\rangle$ locate far above the ground state, about 90 000 cm^{-1}, and one-phton detunings may become very large values around 70 000 cm^{-1}.

$$\Delta\kappa = \frac{\mathcal{N}\hbar}{2\epsilon_0 c}[\omega_1(a_0 - a_1) + \omega_{-1}(a_0 - a_{-1})], \quad (3)$$

where d_i, a_i, and $\mathcal{N}$ are the Raman coupling constant, dispersion constant, and number density of H_2 molecules, respectively [13]. Using Eqs. (1)–(3), we can obtain the large-coherence condition which is required for the maximal conversion with negligible phase slip as follows:

$$|\rho_{ab}| \gg \frac{1}{2}\frac{|\omega_1(a_0 - a_1) + \omega_{-1}(a_0 - a_{-1})|}{\sqrt{\omega_0(\omega_1|d_0|^2 + \omega_{-1}|d_{-1}|^2)}}. \quad (4)$$

By substituting numerical values for the coupling and dispersion parameters and assuming $\omega_0 = 12\,250$ cm^{-1}, we can reach the coherence condition as $|\rho_{ab}| \gg 0.01$.

We numerically calculated the spatial evolution of the coherence solving density matrix equations and one-dimensional wave propagation equations [13]. The pulse width of each driving laser was assumed to be 15 ns (FWHM), corresponding to a Fourier-limit spectral linewidth 30 MHz (FWHM). Figures 1(a)–1(c) display the calculated $|\rho_{ab}|$ versus Raman detuning $\delta\omega = \omega_{ab} - (\omega_0^{(p)} - \omega_{-1}^{(p)})$ at a propagation distance of 100 μm for three driving laser intensities, 180, 130, and 40 MW/cm^2. Note that a large coherence far exceeding $|\rho_{ab}| = 0.01$ is realized at each peak. For a driving intensity 180 MW/cm^2, $|\rho_{ab}|$ takes a peak value of 0.1 at the negative detuning -50 MHz. The observation of coherence peak shift from the zero detuning may be well understood as being due to the adiabatic preparation of the coherence, and, moreover, the negative shift means that the medium adiabatically follows the antiphased eigenstate [5,13]. Actually, the calculation has shown that the medium state evolved at the detuning -50 MHz is described by the antiphased state with a projection certainty larger than 99%. For 130 MW/cm^2, the behavior is essentially the same as that for 180 MW/cm^2, but with a smaller peak of $|\rho_{ab}| = 0.08$. For a weaker driving intensity 40 MW/cm^2, $|\rho_{ab}|$ takes a peak around zero detuning, but it is still possible to realize a large $|\rho_{ab}|$ value of 0.04. This turns out that, for the weaker driving intensity, the adiabaticity may be less important for the large-coherence preparation. Assuming $|\rho_{ab}| = 0.05$, we have estimated the propagation distance for maximal conversion from $sz = \pi/2$ to be about 200 μm.

Solid parahydrogen crystal was grown from liquid phase in an optical cell with two sapphire windows [14]. We prepared a thin crystal with a thickness of 250 μm by adjusting the separation between the windows. Parahydrogen was obtained by converting normal liquid hydrogen using a catalyst at around 14 K, just above the melting point. The purity of parahydrogen was estimated to be greater than 99.9%. The crystal was grown at a temperature of 15 K under a pressure of 30 atm. After the completion of crystal growth, the temperature of the cell was slowly lowered to 4.8 K, the lowest temperature in the present cryogenic system. Obtained crystal was completely transparent without any visible cracks.

Coherence was prepared by driving with two single-mode pulsed lasers: the Ti:sapphire laser at 738 nm [$\omega_0^{(p)}$] and the YAG laser at 1064 nm [$\omega_{-1}^{(p)}$]. Both were injection seeded by cw-single-frequency Ti:sapphire (Coherent 899-29) and YAG (Lightwave Model 126) laser, respectively. Pulse durations were 25 and 14 ns for the Ti:sapphire and the YAG laser outputs, respectively. Both of the laser beams were overlapped temporally and coaxially focused into solid hydrogen with a beam diameter of 0.35 mm. Intensities of both driving lasers were kept equal throughout the experiments. The maximum intensity in the crystal was 180 MW/cm^2, which was limited by the damage of the crystal. The broadband multimode laser for the parametric beating was a free-running Ti:sapphire laser lasing at 12 250 cm^{-1} (818 nm) with a bandwidth of 290($\pm$15) cm^{-1} (FWHM). The broadband beam was applied coaxially to the driving laser beam axis and was focused to the crystal with a diameter of 0.12 mm, so that the parametric beating may occur through the interaction with uniformly prepared coherence.

In Figs. 2(a)–2(c) we display three kinds of SRS sideband spectra obtained by the driving intensity 40 MW/cm^2 and the zero Raman detuning. Spectra (a) and (b) were photographed by dispersing through a Pellin-Broca prism, and spectrum (c) was photographed by a grating spectrometer. Spectrum (a) was obtained with the two driving lasers only. The driving beams are marked by α_0 (738 nm) and α_{-1} (1064 nm). Two anti-Stokes components marked as α_{+1} and α_{+2} are clearly observed. The two components were observed collinearly to the driving beam axis with the

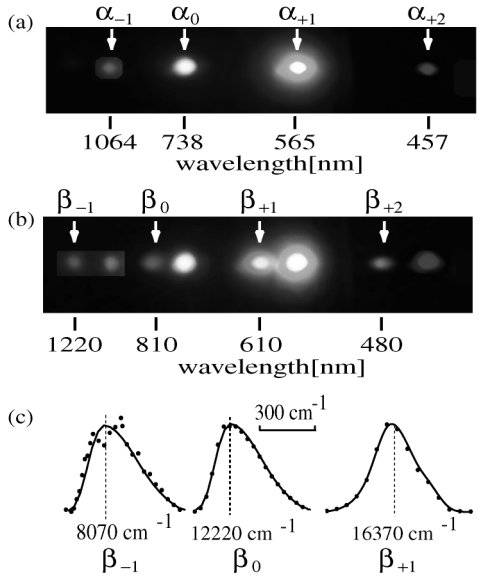

FIG. 2. Sideband spectra dispersed by a prism, (a) and (b), and by a grating spectrometer, (c), with the driving intensity 40 MW/cm^2 and the zero Raman detuning. Sequence α_i is due to the two driving fields only, and sequence β_i due to the applied laser radiation. Half-widths in (c) for β_0, β_{+1}, and β_{-1} components are 290($\pm$15), 280($\pm$15), and 300($\pm$15) cm^{-1}, respectively.

same beam divergence as the incident beams and with a frequency separation corresponding to the $Q_1(0)$ vibrational frequency. Next, we show the Raman sideband spectrum observed by superposing the broadband laser beam to the driving beam axis. The intensity of the broadband laser was 3.3 MW/cm^2. In Fig. 2(b) is displayed the generated sideband spectrum. It is clearly seen that new SRS sequence, β_i ($i = -1$ to $+2$), has been generated with the same frequency separation as the sequence α_i. The β_0 component denotes the applied broadband laser radiation. The β_i sidebands were also observed collinearly on the axis of the laser beams with the same beam divergence as the applied broadband beam. We did not observe any SRS sidebands by using the broadband beam alone. Conversion efficiency (quantum efficiency) from β_0 to $\beta_{\pm 1}$ components reached about 10($\pm$3)% for each at this driving intensity. We estimated the magnitude of coherence from the conversion efficiency to be $|\rho_{ab}| \sim 0.02$. Spectral profiles for β_i ($i = -1$ to 1) components are displayed in Fig. 2(c). Note that the broadband nature of the multimode laser is exactly replicated to the Raman sidebands: half-widths for the β_{+1} and β_{-1} components are 280($\pm$15) and 300($\pm$15) cm^{-1}, respectively, exhibiting good agreement with the width for the applied beating beam β_0, 290($\pm$15) cm^{-1}. For stronger driving intensities, the spectral profile was replicated also as those in the figures but with higher conversion efficiencies.

Tuning characteristics for the α_{+1} and β_{+1} components are displayed in Figs. 3(a)–3(f) for three driving intensities, 130, 40, and 10 MW/cm^2. The Raman detuning was

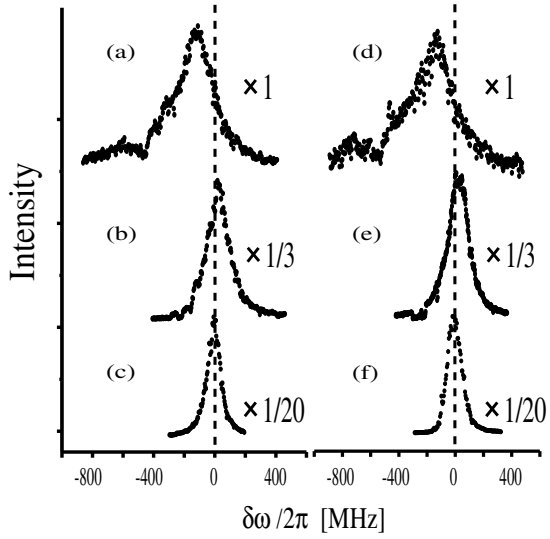

FIG. 3. Tuning characteristics for two Raman sideband components, α_{+1} and β_{+1}, for three driving laser intensities. Each peak is scaled to the same value. Traces (a)–(c) are for α_{+1} component, and traces (d)–(f) are for β_{+1} component. Traces in (a) and (d), in (b) and (e), and in (c) and (f) are for the driving intensities, 130, 40, and 10 MW/cm^2, respectively.

controlled by tuning the single-mode Ti:sapphire laser. In order to monitor the Raman resonance, we simultaneously measured the SRS tuning characteristics in a weak pump limit for each measurement by passing a fraction of the driving beams to a different portion of the solid hydrogen from the strongly driven region. The Raman resonance was detected through an observation of the α_{+1} component at 565 nm using a photomultiplier through a monochromator. As seen in the figures, the tuning characteristics are exactly the same for the α_{+1} and β_{+1} component. This shows that the broadband parametric replication is due to the Raman coherence prepared by the two single-mode driving lasers. The traces clearly show that the tuning curves become broader and asymmetric to the Raman resonance with the increase of the driving intensities, and one can readily recognize that the essential features of the experimental observations well correspond to the calculated behaviors of coherence displayed in Fig. 1. For the driving intensity of 10 MW/cm^2, the generation occurs around the Raman resonance over 100 MHz bandwidth with symmetric profile, and for 40 MW/cm^2 driving intensity the peak still locates at the Raman resonance. For the intensity of 130 MW/cm^2, the peak shifts to a negative side with the Raman detuning of -120 MHz, and most of the parametric generation occurs on the negative side.

Figure 4(a) displays the conversion efficiency (quantum efficiency) from the applied beating laser to the β_{+1} component versus the beating laser intensity. The driving intensity was fixed to 40 MW/cm^2, and the Raman detuning was set to zero. Intensity of the β_{+1} component was obtained by measuring both energy and temporal

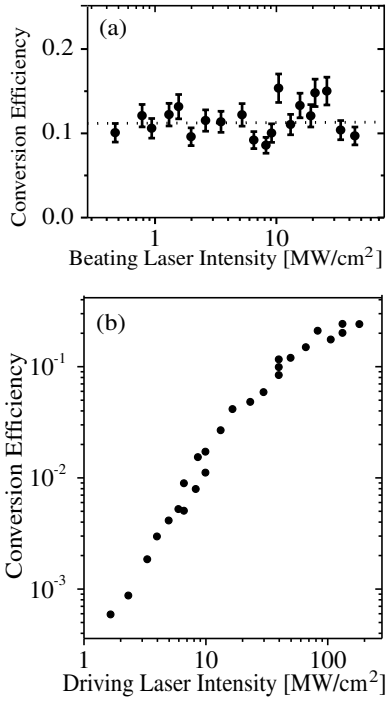

FIG. 4. Conversion efficiency (quantum efficiency) from beating laser to β_{+1} sideband; (a) is versus the beating laser intensity. Driving intensity was fixed to 40 MW/cm^2. Raman detuning was set to zero. (b) is versus the driving laser intensity. Beating laser itensity was fixed to 3.3 MW/cm^2. Raman detuning was set to $\delta\omega/2\pi = -120$ MHz.

profile. Although the beating laser intensity is varied about two order, the conversion efficiency is constant within the experimental errors. This confirms again that the present sideband generation process is the coherent beating process due to the prepared Raman coherence. Figure 4(b) displays the conversion efficiency versus the driving laser intensity. The beating laser intensity was fixed to 3.3 MW/cm^2, and the Raman detuning was set to -120 MHz. With the increase of the driving laser intensities until 10 MW/cm^2, the conversion efficiency is quadratically enhanced, and it almost saturates at about 100 MW/cm^2, that is a clear signature of reaching the maximal conversion condition. Conversion efficiency reaches a maximum value $24(\pm 5)\%$ at the driving intensity 180 MW/cm^2. The conversion efficiency for the β_{-1} component exhibited the same behavior as that for the β_{+1} component with maximum conversion efficiency of $30(\pm 10)\%$ at 180 MW/cm^2. These observations mean that the prepared coherence has replicated the applied broadband laser photons to the collinearly propagating $\beta_{\pm 1}$ Raman sidebands by a total conversion efficiency of about 50% with a propagation distance of 250 μm. Through a comparison with the numerical simulations we have estimated the realized coherence as $|\rho_{ab}| \sim 0.05$ at the Raman detuning -120 MHz, which far exceeds the requirement for the large coherence.

In summary, we have demonstrated the collinear parametric Raman sideband generation using solid hydrogen. We have shown that the Raman coherence strongly driven with two single-mode lasers beats with multimode laser radiation with very broad bandwidth, and efficiently replicates the broadband nature to the Raman sidebands with a signature of saturation. We have also shown that the sideband generation occurs mainly on the negative side of Raman detuning, where the medium may adiabatically follow the antiphased state.

The authors thank M. Suzuki for his contributions on low temperature experiments.

*Permanent address: Department of Physics, University of Hanoi, Hanoi, Vietnam.

[1] S. E. Harris, Phys. Today **50**, 36 (1997).
[2] S. E. Harris, G. Y. Yin, M. Jain, H. Xia, and A. J. Merriam, Philos. Trans. R. Soc. London A **355**, 2291 (1997).
[3] M. Jain, H. Xia, G. Y. Yin, A. J. Merriam, and S. E. Harris, Phys. Rev. Lett. **77**, 4326 (1996); A. J. Merriam, S. J. Sharpe, H. Xia, D. Manuszak, G. Y. Yin, and S. E. Harris, Opt. Lett. **24**, 625 (1999).
[4] A. S. Zibrov, M. D. Lukin, and M. O. Scully, Phys. Rev. Lett. **83**, 4049 (1999).
[5] S. E. Harris and A. V. Sokolov, Phys. Rev. Lett. **81**, 2894 (1998).
[6] D. D. Yavuz, A. V. Sokolov, and S. E. Harris, Phys. Rev. Lett. **84**, 75 (2000).
[7] K. Hakuta, M. Suzuki, M. Katsuragawa, and J. Z. Li, Phys. Rev. Lett. **79**, 209 (1997); K. Hakuta, M. Katsuragawa, and M. Suzuki, Philos. Trans. R. Soc. London A **355**, 2405 (1997).
[8] A. V. Sokolov, D. R. Walker, D. D. Yavuz, G. Y. Yin, and S. E. Harris, Phys. Rev. Lett. **85**, 562 (2000).
[9] J. Van Kranendonk, *Solid Hydrogen* (Plenum, New York, 1983).
[10] D. P. Weliky, T. J. Byers, K. E. Kerr, T. Momose, R. M. Dickson, and T. Oka, Appl. Phys. B **59**, 265 (1994).
[11] J. Z. Li, M. Katsuragawa, M. Suzuki, and K. Hakuta, Phys. Rev. A **58**, R58 (1998).
[12] M. Katsuragawa and K. Hakuta, Opt. Lett. **25**, 177 (2000).
[13] Fam Le Kien, J. Q. Liang, M. Katsuragawa, K. Ohtsuki, K. Hakuta, and A. V. Sokolov, Phys. Rev. A **60**, 1562 (1999).
[14] M. Suzuki, M. Katsuragawa, R. S. D. Sihombing, J. Z. Li, and K. Hakuta, J. Low Temp. Phys. **111**, 463 (1998).